Title:

System and Material Parameter Effects on Thermoelectric Power Generation in Three Combustion Systems

Authors:

Saniya LeBlanc[1] and Kenneth E. Goodson

Department of Mechanical Engineering, Stanford University, Stanford, California 94305, USA

[1]Corresponding author

Email: sleblanc@stanford.edu

Tel: +1 (202) 256-5874

Fax: +1 (650) 723-7657

440 Escondido Mall

Bldg. 530, Rm. 224

Stanford, CA 94305

USA

Abstract:

Thermoelectric cogeneration offers an opportunity to recover waste heat from a variety of combustion systems. Computationally efficient simulations of practical systems that allow optimization and illustrate the impact of key material and system parameters are necessary. This work compares differences in thermoelectric material conversion efficiency and system-level power generation by simulating three combustion systems: a water heater, an automotive exhaust system, and an industrial furnace. A more detailed simulation for a 15 kW tankless, methane-fueled water heater further explores the potential for small-scale, stationary cogeneration. The simulation uses the finite volume method and links convective flow in a compact heat exchanger and conduction through the system to determine thermoelectric power generation. For a single water heater pipe, 126 W of electrical power can be generated, and a typical system could yield 370 W. While varying thermoelectric material parameters such as thermal conductivity can improve thermoelectric output by over 50%, system components like thermal interface materials can severely limit power output. The impact of thermal interface resistance on power generation efficiency is established for all three combustion systems. The analysis demonstrates the impact system parameters have on the feasibility of thermoelectric waste heat recovery in combustion systems.

NOMENCLATURE

A	heat transfer area
C_p	heat capacity
h	convection coefficient
I	current
k	thermal conductivity of TEM material
$\dot{m}$	mass flow rate
P	electrical power from TEM
q_g	heat transfer rate from gas stream
q_{Joule}	Joule heating
$q_{Peltier}$	heat transfer due to Peltier effect
q_{TEM}	heat transfer rate through TEM
q_w	heat transfer rate to water stream
R_{load}	electrical resistance of load
R_{pw}	thermal conduction resistance of pipe wall
$R_{TEM,e}$	electrical resistance of TEM
R_{th}	thermal interface resistance
S	Seebeck coefficient
$T_{g,i}$	gas inlet temperature
$T_{g,o}$	gas outlet temperature
T_p	exterior pipe wall temperature
T_{pw}	interior pipe wall temperature
t_{TEM}	TEM thickness

$T_{TEM,c}$ TEM cold side temperature

$T_{TEM,h}$ TEM hot side temperature

T_w water temperature

Z thermoelectric figure of merit

Greek symbols

ε heat exchanger effectiveness

ΔT_{lm} log mean temperature difference

ΔT_{TEM} temperature difference across TEM

ρ electrical resistivity

η_o total fin surface efficiency

η_{TE} module thermoelectric conversion efficiency

η_{sys} system thermoelectric conversion efficiency

σ_{TE} parasitic heat loss

1. Introduction

Heat losses reduce the efficiency of combustion systems. Thermoelectric modules (TEMs) operating as power generators can improve system efficiency using the waste energy available in combustion products [1, 2]. Thermoelectric generators are attractive cogeneration solutions because they are reliable, silent, and have no moving parts. Moreover, they offer the benefit of generating electricity locally at distributed combustion facilities or even household units, diminishing the need to draw power from a distant plant [3]. Extensive effort has been focused on utilizing waste heat for thermoelectric energy conversion [4, 5]. Applications include automobiles, high-temperature electronics, and gas-powered appliances used by individuals or small groups. Thermoelectric generators can also be used in systems such as water heaters in which the goal is to transfer heat energy [6, 7].

Thermoelectric materials [8] and systems with incorporated TEMs [9-11] have been previously investigated. Maximizing thermoelectric material efficiency is different than maximizing the power output of a TEM integrated into a system [12]. Extensive research has focused on improving TEM performance through the figure-of-merit, $ZT = S^2T/\rho k$, of thermoelectric materials where S, ρ, and k are the Seebeck coefficient, electrical resistivity, and thermal conductivity of the thermoelectric material, respectively. The temperature-dependent properties are evaluated at the average temperature T within the TEM. There has been considerable effort to develop phonon-glass/electron-crystal materials to reduce thermal conductivity while maintaining high values of electrical conductivity. Efforts to control the crystal structure of bulk thermoelectric materials as well as develop nanostructured materials to increase phonon scattering and improve ZT are ongoing [13]. However, maximizing Z is not necessarily the best method to optimize an entire cogeneration system. For example, combustion systems and robust electronic systems experience high operating temperatures and large temperature fluctuations, but the efficiency of many thermoelectric materials rapidly declines at high

temperatures. The realization of practical, effective cogeneration systems hinges on investigating the impact of thermoelectric material parameters coupled with system parameters.

A major challenge with system development is inefficiency caused by temperature drops at interfaces which are quantified using thermal interface resistances (TIRs) [14]. Wide temperature fluctuations, frequent thermal cycling, and large contact area in thermoelectric systems both degrade the performance of traditional thermal interface materials (TIMs) and make the module more susceptible to device failure from thermal expansion mismatch. Possible damage from thermal expansion also limits the rate of temperature change in a TEM. Nano-structured thermal interfaces, including those incorporating aligned carbon nanotubes (CNTs) or metal nanowires, may lead to improved reliability. Previous work has shown that CNT arrays may perform as an exceptional thermal interface material because they have both high thermal conductivity and mechanical compliance [15-19].

The current work estimates representative thermoelectric power generation capabilities for home water heater, automotive exhaust, and industrial furnace waste heat recovery. The goal is to compare material thermoelectric conversion to system power generation by accounting for components such as interface layers and heat exchangers. Distributed, stationary thermoelectric power generation is explored with a detailed simulation of a 15 kW, methane-fueled, tankless water heater. This work investigates TEM output when both material properties and system parameters are considered. Varying thermal interfaces and the potential of novel TIMs are presented. The limiting nature of thermal resistances in a thermoelectric cogeneration system is demonstrated, and system optimization is informed by varying parameters. The impact of thermal interface resistance on power generation efficiency is compared for water heater, automotive exhaust, and industrial furnace waste heat recovery.

2. Multi-system comparison

A compact, parametric system model enables a comparative analysis of three relevant thermoelectric heat recovery applications: a home water heater, an automotive exhaust system, and an industrial furnace. A home water heater represents the potential for small-scale, stationary energy harvesting. In automobiles, roughly 40% of fuel energy is wasted as heat [20], so thermoelectric conversion of automotive exhaust heat offers an opportunity for improved fuel economy and reduced environmental impact, especially considering the scale of the worldwide automotive sector. Industrial waste heat recovery with thermoelectrics has received increasing attention since many industrial processes such as metal and glass melting discharge gas at high temperatures [21]. Thermoelectric energy harvesting offers an opportunity for energy efficiency through on-site electricity generation for these large-scale, stationary applications.

Simulation of thermoelectric systems reveals the relationship between system parameters and their impact on efficiency and power generation in these three applications. Figure 1 depicts a system with hot exhaust and coolant fluid streams flowing through heat exchangers surrounding a thermoelectric module. Figure 2 provides a thermal circuit model for the system including the temperatures of the hot gas stream and the coolant stream as nodes. Many thermoelectric system studies recognize the significant distinction between TEM conversion efficiency and overall system efficiency [22, 23]. Fewer studies consider the critical role system parameters such as thermal interface resistance, heat exchanger effectiveness, and mass flow rate play in thermoelectric power generation capabilities of combustions systems [24, 25]. A compact model assuming fixed hot and cold stream temperatures while including the impact of heat exchangers, parasitic heat loss, and interface resistance has been developed [25]. By fixing the hot and cold stream temperatures to the inlet temperatures, the spatial temperature variation along fluid flow directions is eliminated [23, 25, 26]. Although this approximation overestimates the overall temperature gradient and thus the power generation potential, this approach enables rapid multi-system comparisons.

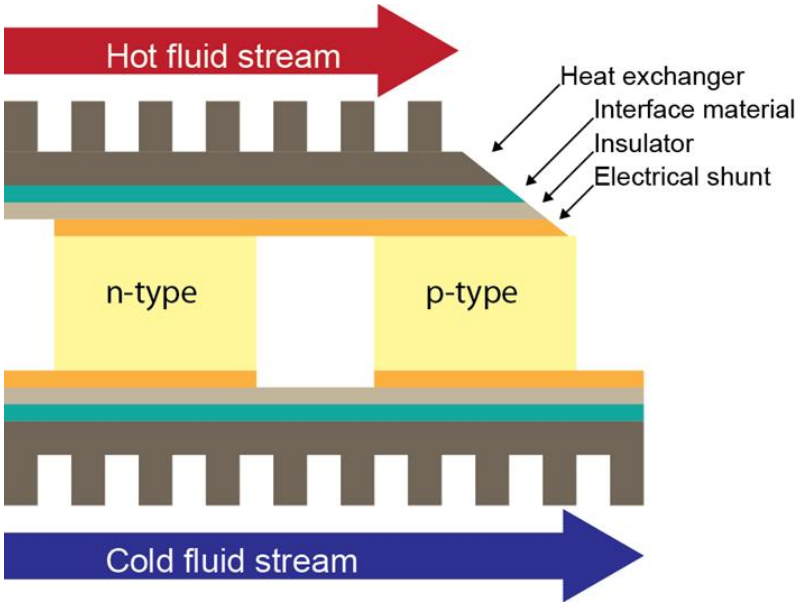

Figure 1. A thermoelectric system has multiple n- and p-type legs connected electrically in series with an electrical shunt material. An electrical insulator surrounds the TEM, and a thermal interface material connects the TEM to heat exchangers. Heat flows from the hot stream to the cold stream through the TEM with the thermoelectric legs connected thermally in parallel.

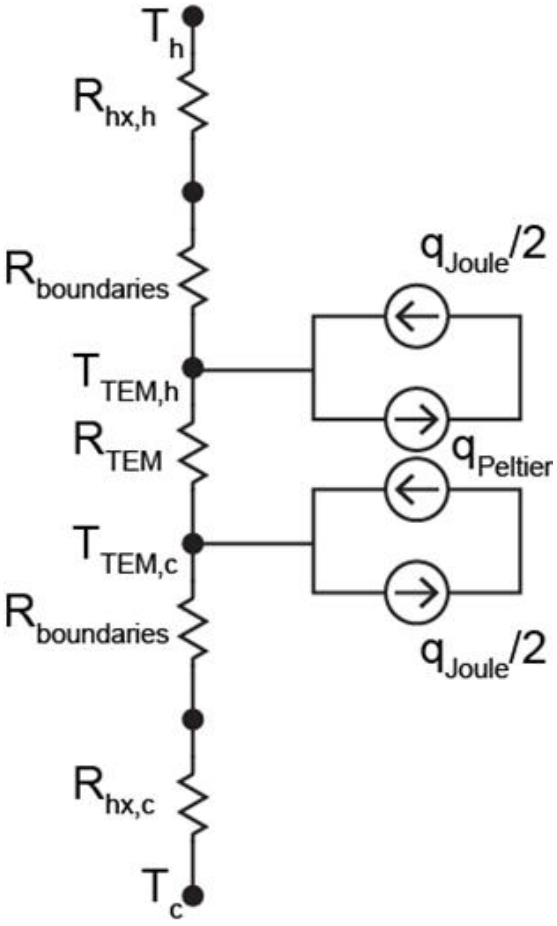

Figure 2. The thermoelectric system can be represented by a thermal circuit in which heat flow from the hot source through the system to the cold sink. The boundaries include conductor, insulator, and thermal interface material.

A system of equations describing the heat flow, power generation, and conservation of energy can be solved to determine conversion efficiencies. As indicated in Figure 2, the heat transfer through the TEM must account for Joule heating and the Peltier effect in addition to conduction through the TEM:

$$q_{Joule} = I^2 R_{TEM,e} \quad (1)$$

$$q_{Peltier} = ST_{TEM,h,c}I \tag{2}$$

$$q_{TEM} = \frac{k_{TEM} A\left(T_{TEM,h} - T_{TEM,c}\right)}{t_{TEM}} \tag{3}$$

The Peltier heat flux is dependent on the temperature of each side of the TEM. The temperature gradient through the TEM determines the electrical potential developed across it. The electrical power obtained from the TEM once it is connected to a load resistor is

$$P = I^2 R_{load} = I(S\Delta T_{TEM} - IR_{TEM,e}) \tag{4}$$

where the product of the Seebeck coefficient and temperature difference is the voltage drop. For a maximum power generation condition where the load and TEM electrical resistances are matched, the thermoelectric conversion efficiency is [25]

$$\eta_{TE,P} = \frac{P_{\max}}{q_h} = \frac{S^2\left(T_{TEM,h} - T_{TEM,c}\right)^2 \Big/ 4R_{TEM,e}}{\left[\frac{\left(T_h - T_{TEM,h}\right)\left(1-\sigma_{TE,h}\right)}{\left(\dot{m}_h C_{p,h}\varepsilon_h\left(1-\sigma_{ex,h}\right)\right)^{-1} - R_{th,h}}\right]} \tag{5}$$

The heat flow into the TEM from the heat exchanger, q_h, shows the pertinent system parameter dependencies. An energy balance on the TEM cold side is similar for the heat flow out of the TEM, q_c, and an energy balance around the TEM shows $q_h = P_{gen} + q_c$. The terms σ_{TE} and σ_{ex} represent the fractional heat loss to the environment at the TEM and heat exchanger, respectively. These terms generally have minimal impact and are neglected here, but they can be considerable in specialized applications [27]. Thermal interface resistance R_{th} is present on both sides of the TEM where the TEM attaches to the heat exchangers. The heat exchanger effectiveness ε is obtained from ε-*NTU* (number of transfer units) relationships [28]. The overall system efficiency η_{sys} is the electrical power generated divided by the maximum energy that could be transferred from the hot exhaust stream.

Realistic parameters were modeled by using data reported for operation of each system: a water heater (reported here), a sports-utility vehicle [11], and an oxy-fuel glass processing furnace [21]. The parameters used in the model are listed in the appendix. It will take a number of years for thermoelectrics technology to penetrate these applications. In the meantime, thermoelectrics materials research is advancing at a rapid pace, and improved material properties are inevitable. This development was accommodated by selecting recently reported temperature-dependent property data for nanostructured PbTe [29].

The model was used to compare the difference between TEM efficiency and overall system efficiency. Ideal efficiency values are presented in Table 1 for the three systems indicated. The system efficiency is 32%, 33%, and 59% lower than thermoelectric conversion efficiency for the water heater, automotive exhaust, and industrial furnace applications, respectively.

Table 1. Thermoelectric module and system efficiencies for three simulated combustion waste heat recovery systems were determined. Thermal interface resistance and parasitic heat loss values were omitted to obtain

upper limits. Optimal heat exchanger effectiveness reported in previous studies was included as indicated in the supplementary information.

System	η_{TE}	η_{sys}	η_{sys} / η_{TE}
Water heater	4.6%	3.2%	0.68
Automobile	2.1%	1.4%	0.67
Industrial furnace	12%	4.8%	0.41

These results are promising for small-scale, distributed applications like the water heater since a reasonable efficiency is achievable. Industrial furnace exhaust heat recovery is likely to receive increasing attention since the efficiency is acceptable, and the potential to offset industrial electricity use is attractive. While the automotive exhaust system converts the available thermal energy less effectively, consideration of only a performance analysis like this is misleading. The latter two systems benefit from economies of scale, and an evaluation of performance coupled with cost provides a more valid assessment of thermoelectric waste heat recovery potential [30, 31].

3. Detailed analysis of the water heater application

Efficiency improvements for appliances such as water heaters, refrigerators, and furnaces are both financially and environmentally cost-effective [32]. Deeper insight into the factors affecting thermoelectric waste heat recovery requires a more detailed analysis than the approximate calculations performed above. Such analyses have been conducted for automotive exhaust heat recovery applications [33, 34]. This approach can require detailed iterative schemes, hampering the ability to evaluate a range of parameters and compare multiple systems as accomplished above. However, it provides spatial resolution of thermal gradients which is essential for system and TEM optimization [22]. The analysis below refines the water heater system model to link thermoelectric power generation to heat transfer physics in a cross-flow heat exchanger setup.

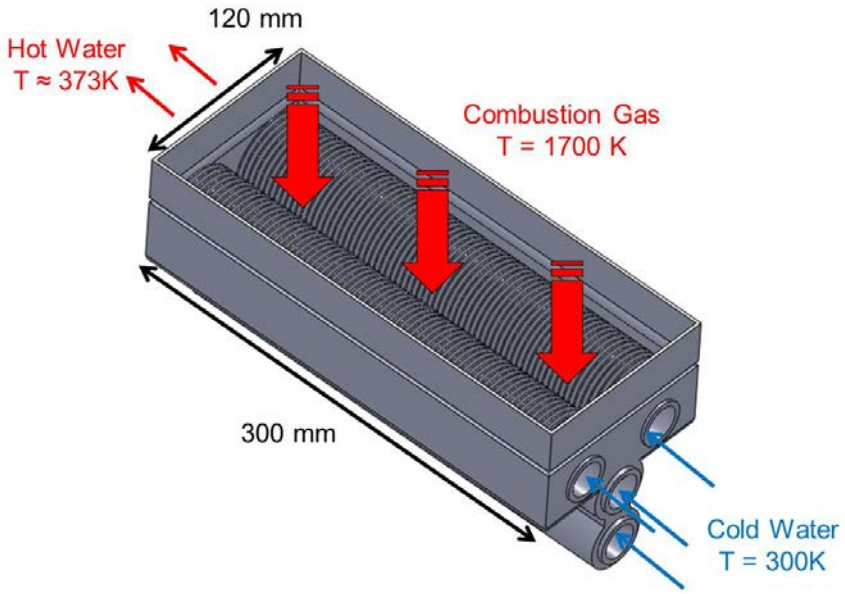

Figure 3. A combustion gas stream flows through a cross-flow heat exchanger to heat water in a tankless water heater system. The pipe length, inner diameter, and outer fin diameter are 300 mm, 30 mm, and 60 mm, respectively.

A numerical simulation of a tankless water heater system is conducted to indicate the possibility of efficiency improvement through thermoelectric heat recovery. Also termed demand or instantaneous water heaters, tankless water heaters use a heat source to directly heat cold water without storing water in a tank and incurring energy loss [35, 36]. Figure 3 shows the water heater system with a fluid cross-flow arrangement through an annular-finned pipe. A water heater system has multiple pipes like the one shown. This practical heat exchanger setup is used in many applications in which cogeneration may be feasible. The thermoelectric module is modeled as a ring-shaped structure to match the pipe's shape [37]. The surface is fully covered by thermoelectric material. Optimization of fractional area coverage, or fill factor, has been investigated elsewhere [30]. The thermoelectric material is surrounded by an electrical conductor, a ceramic insulating layer, and a

thermal interface material to connect the TEM to the pipe. The model accounts for external gas convection, heat generation by the TEM, and the flow rate dependence of the convection coefficients.

The external and internal convection components use empirical correlations to determine the average convection coefficients. The heat transfer from the gas stream is determined using

$$q_g = \left[\frac{1}{\eta_o h_g A} + R_{pw} \right]^{-1} \Delta T_{lm} \tag{6}$$

to account for the effective fin efficiency of the annular pipe wall fins and the cylindrical wall conduction resistance [28]. The average gas convection coefficient is determined from a correlation for a compact heat exchanger with circular finned pipes [38]. The driving temperature difference between the gas and the pipe is approximated using a log mean temperature relationship:

$$\Delta T_{lm} = \frac{\left(T_{g,o} - T_p\right) - \left(T_{g,i} - T_p\right)}{\ln\left(\frac{T_{g,o} - T_p}{T_{g,i} - T_p}\right)} \tag{7}$$

Integrating the local heat transfer rate between two fluids over the total heat exchange area leads to a logarithmic relationship between the temperature differences. Modeling the temperature gradient this way allows a close approximation of the pipe wall temperature and its variation in the water flow direction without requiring a detailed solution of the temperature profile in the pipe wall along the gas flow direction. The heat transfer rate from the interior pipe wall to the water stream is

$$q_w = h_w A\left(T_{pw} - T_w \right) \tag{8}$$

where h_w is determined from the correlation for laminar internal flow [28].

The simulation results show the temperature range around the TEM is 400 K to 600 K. The chalcogenide lead telluride is an optimal thermoelectric material at these operating temperatures, so the standard properties of PbTe are used initially to explore the option of a near-term solution which does not rely on new materials development [39]. Optimal properties are selected to mimic the ability of segmented thermoelectric legs to maximize energy conversion [40]. Thermal and electrical interface resistances are neglected to ascertain upper bounds.

The simulation is conducted using a finite volume method. Each pipe is discretized in the longitudinal direction. A shooting method is used to determine the water temperature for each volume. The water temperature is assumed to be a mixed mean temperature representing the entire discrete volume. A false position or *regula falsi* method allows convergence on the amount of heat transferred to the water. Conservation of energy analyses on the results verified the simulation technique. This simulation approach is simpler than a finite element model, and it captures the significant thermal and electrical physics of the system. The approach reveals key parameters and their relative significance in system optimization.

In order to isolate the influence of system and TEM parameters, a single pipe of a tankless water heater system is simulated initially; system specifications are provided in the supplementary information. Figure 4 summarizes a single pipe simulation result. In 4a, the change in fluid temperatures demonstrates energy exchange between the hot gas and the water. The gas and the water do not reach the same temperature before the water exits the pipe, indicating additional thermal energy is available for harvesting. For cases of longer pipe length or lower water flow rate, the change in temperature with distance would decrease. The temperature drop across the TEM along the length of the pipe decreases, so the voltage developed across the TEM

diminishes. In optimizing a system, the change in temperature drop indicates the thermoelectric material could vary along the length of the pipe since the thermoelectric figure of merit *ZT* is temperature dependent.

Figure 4b depicts the total electrical power from the TEM as a function of current through it. Current and load resistance are inversely related, so increasing current corresponds to decreasing load resistance. The peak power output occurs where the load resistance is equal to the electrical resistance of the TEM. The average gas outlet temperature declines as more heat energy is converted to electrical energy. The water outlet temperature changes minimally because the product of mass flow rate and specific heat capacity is larger for the water stream than the gas stream. The ability to obtain the maximum electrical power output without significantly reducing the water output temperature is promising.

Optimal system operating points are influenced by considering both conversion efficiency and relative gain in TEM power with changing load resistance. The electrical power from the TEM can be divided by the energy transferred into the system from the hot gas minus the amount of energy transferred to the water to obtain a non-dimensional power value. For a single pipe, this non-dimensional power peaks at 0.8% with an average gas outlet temperature of 1100 K indicating a significant amount of energy that can still be harvested from the gas. The voltage developed across the TEM is dropped across the TEM electrical resistance and an external load resistance. While the electrical power output comes from the voltage drop across the load resistor, the power dissipated in the TEM contributes to Joule heating and can be beneficial in this system to heat the water. The ratio of TEM power output to power dissipated decreases from an initial amount of 21 to 1 at the matched load condition. This corresponds to an initial incremental increase in electrical power of 6.8 W/A, and the increase in power per unit rise in current declines to zero at 37 A. Because the increase in incremental TEM output power diminishes, the optimal operating point may not be at the peak power condition [25].

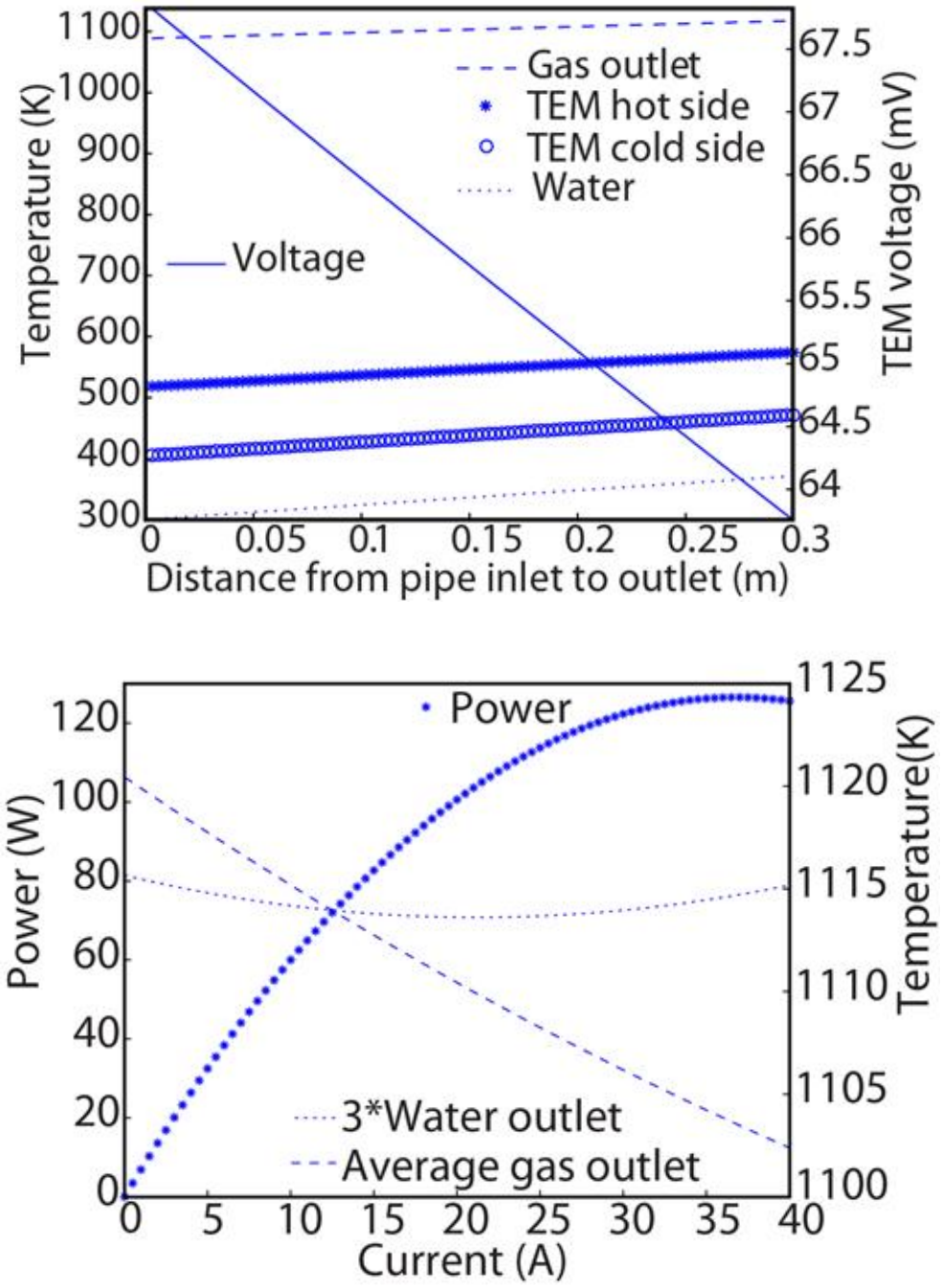

Figure 4. a) Fluid temperatures, TEM boundary temperatures, and TEM voltage are determined as a function of distance along the pipe. b) Electrical power output from the TEM corresponds to a change in gas and water outlet temperatures. The maximum power output for the simulated single pipe heat exchanger is 126 W.

The impact of varying system and TEM parameters are determined. Figures demonstrating the impact of flow rate, convection coefficients, and Seebeck coefficient are provided in the supplementary information, and the results are summarized here. Thermoelectric power output rises as the flow rate of the water stream due to increased convective cooling of the pipe wall resulting in a larger temperature drop across the TEM. Modifying the gas convection coefficient h_g mimics multiple system variations. For example, altering fin geometry or gas flow rate will change h_g. Doubling the convection coefficient can increase the electrical power output by 50%, and the value of h_g affects the impact of the gas side convective thermal resistance relative to the other system thermal resistances. The convective resistance is often the highest heat transfer resistance [9]. This work indicates the gas side convective resistance can be comparable to TEM resistance as TEM thickness increases. The relative importance of interface resistance increases as the gas side convection improves. The limiting effect of interface materials is discussed in more detail below.

Altering the TEM thermal conductivity is an effective way to increase output power; the power is more than doubled if the thermal conductivity is reduced by 1 W/m-K. Of all the parameters considered, thermal conductivity improvement results in the largest gain in power output. The top axis in Figure 5 shows *ZT* corresponding to varying thermal conductivity with all other properties held constant. The maximum operating temperature of the thermoelectric material must be considered in evaluating the *ZT* and selecting TEM materials. For example, Bi_2Te_3 has a maximum operating temperature of about 550 K and could not be considered for this application.

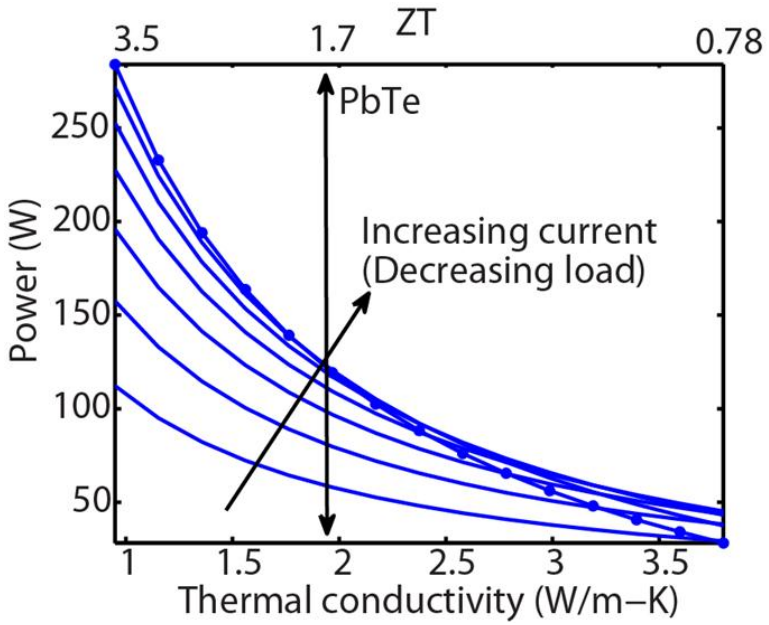

Figure 5. TEM electrical power output increases significantly as thermoelectric material conductivity decreases. Optimized materials are simulated by holding the other material properties constant. The curve for the lowest load resistance has markers to guide the eye.

The maximum electrical power output depends on the configuration of the heat exchanger system. Options for pipe configurations in the water heat system are considered in Table 1. The table provides the incremental gain in adding pipes in multiple configurations. Pipes located next to each other horizontally are in a parallel thermal connection whereas vertically stacked pipes are in a series thermal connection. The gas outlet temperature is indicative of the amount of energy remaining in the gas stream after it has passed over all of the pipes. Because the gas stream temperature drops as it passes over the pipes, the electrical power out of a pipe's TEM decreases as it is stacked lower in a vertical arrangement. However, increasing the number of pipes stacked horizontally would also require an increase in the mass flow rate of the gas stream. Additionally, the average temperature across the TEM is significantly different in each pipe, so different thermoelectric materials

should be considered. The TEM material in each pipe should have a peak *ZT* for the operating temperature of that pipe.

Table 2. Systems configurations can vary to connect pipes thermally in parallel and series. TEM electrical output increases most for parallel arrangements at the cost of higher gas flow rates.

Pipe configuration	Diagram of cross-section	Peak power output (W)	Gas outlet temperature (K)	Thermal connection
Single		250	1100	2 pipes in parallel
4 horizontal, stacked	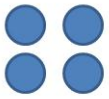	340	740	2 parallel sets with 2 in series
6 horizontal, stacked	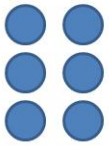	370	530	3 parallel sets with 3 in series
4 horizontal *requires higher gas flow rate		500	1100	4 in parallel

4. Impact of thermal interfaces

Estimating the thermal resistance of interface materials is a major challenge for this work. Interface materials from thermal greases to metallic alloys have thermal conductivities ranging from 0.2 to 50 W/m-K [41]. In modern computers, these materials have thicknesses between 20 and 100 μm, yielding total thermal resistances from 150 to 0.6 m^2K/MW. In macroscale systems such as a water heater the thicknesses of interface materials can be substantially larger. The large thickness is owed to geometrical inconsistencies in the larger

components as well as the requirement for the interface to overcome thermomechanical mismatch between the adjacent materials. In contrast to computers, which are subjected to a temperature variation of approximately 100 K, combustion-based TEM systems could experience thermomechanical cycling up to 600 K. For the present work, we assume a TIM thickness of 1 mm and thermal conductivities of 1 W/m-K for grease, 10 W/m-K for metal solder, and 100 W/m-K for a novel CNT-based interface material [16, 18].

The degree to which thermal interface resistance degrades system efficiency depends strongly on thermoelectric thickness. Figure 6 illustrates a thicker TEM raises the TEM thermal resistance and thus the temperature drop across it. A 22 W/mm improvement in power is possible. The thermal interface material strongly reduces the output power and severely affects power output as TEM thickness increases. Particularly for TEMs composed of novel thin film materials, power generation capability will be limited by the heat sink and TIM thermal resistances, and thermal resistance matching between these system elements and the TEM is critical [42].

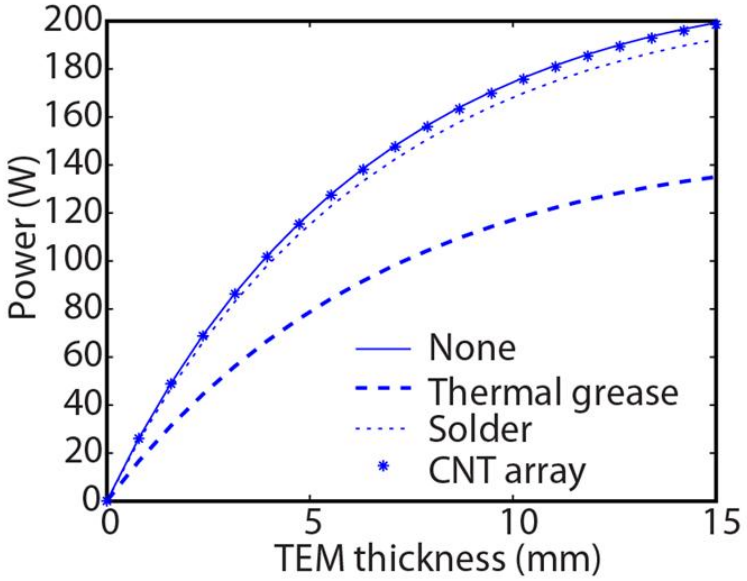

Figure 6. TEM electrical power output increases with TEM thickness, but interface materials can severely limit the gain in power output. An interface material thickness of 1 mm is used for the simulation.

As shown in Figure 1, there are two thermal interfaces, one on each side of the thermoelectric module. Hot side TIR is higher than cold side TIR in practical systems, so the analysis is extended to account for $R_{th,h}$ equal to and multiple factors larger than $R_{th,c}$. The values of $R_{th,c}$ shown in Figure 6 correspond to TIMs with thermal conductivity from 1 to 100 W/m-K, and the solid line shows the maximum operating point with no TIR.

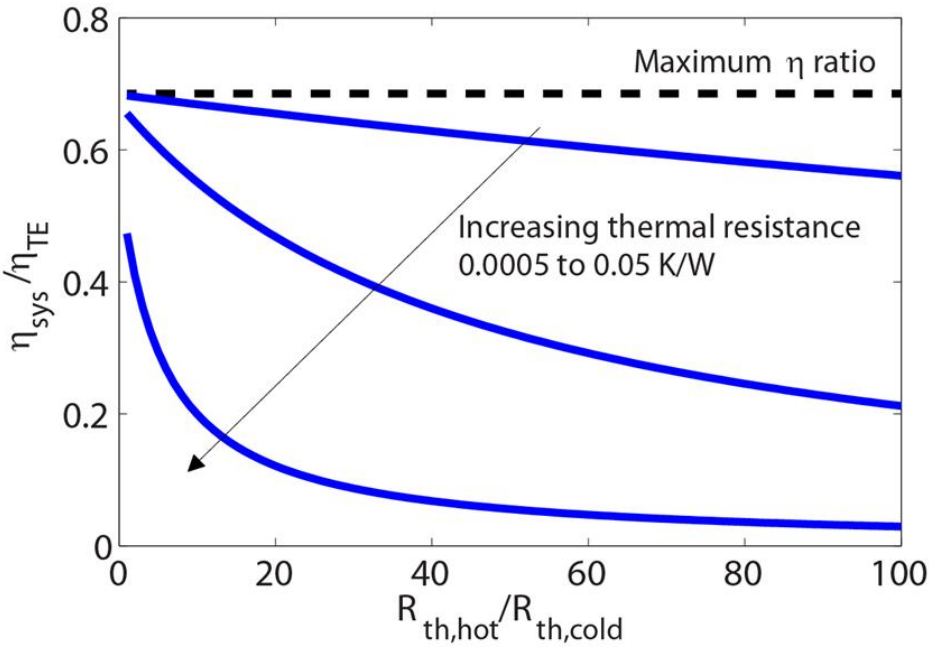

Figure 7. The ratio of system to module thermoelectric conversion efficiency is compared to the ratio of hot side to cold side thermal interface resistance for the water heater system. The efficiency reduction decreases as the thermal interface resistance decreases.

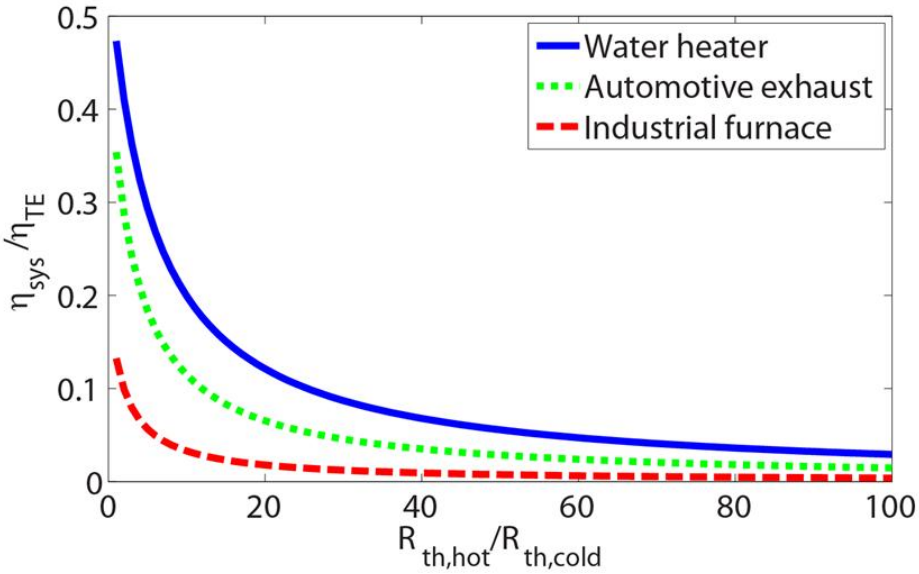

Figure 8. The ratio of system to module thermoelectric conversion efficiency is compared to the ratio of hot side to cold side thermal interface resistance for the three combustion systems. The relationship can be fit to an exponential decay to characterize the efficiency reduction due to the interfaces. $R_{th,c}$ is held constant at 0.05 K/W.

The severe degradation in power generation potential due to thermal interface resistance is not limited to appliance-type systems like the water heater. Figure 7 illustrates the impact of TIR for all three applications: water heater, automotive exhaust, and industrial furnace. The relationship between the efficiency and TIR ratios is of the form

$$\frac{\eta_{sys}}{\eta_{TE}} = ae^{b\left(R_{th,h}/R_{th,c}\right)} + ce^{d\left(R_{th,h}/R_{th,c}\right)} \tag{9}$$

where a,b,c, and d are coefficients dependent on $R_{th,c}$. This analysis provides rapid assessment of TIM system-level impacts. It is much easier to measure the effective TIR for TIMs at lower temperatures. Experimental

setups to measure TIMs at high temperatures (e.g. exhaust stream temperatures of these systems) are rare and challenging to develop [43]. Using this analysis, an easily obtained value of $R_{th,c}$ can be combined with an estimate of the relative $R_{th,h}$ value to determine the effects of system efficiency reduction due to thermal interface resistances.

5. Conclusion

The difference between thermoelectric material conversion efficiency and system-level power generation in three combustion applications is determined. A tankless water heater system with an integrated thermoelectric module is numerically simulated in detail to investigate the impact of varying both system and TEM parameters. Reducing the TEM thermal conductivity by 50% doubles the electrical power output. Increasing the hot side convection coefficient and increasing the TEM thickness can increase the output power by up to 50%. Thermal interface materials significantly limit the ability of a TEM to maximize output in a cogeneration system. Industry standard TIMs can reduce TEM power output by approximately 40% depending on material and thickness. More work is needed to minimize this thermal resistance while accounting for the severe repetitive thermomechanical cycling in these systems. The current work suggests that novel interfaces such as those based on CNT technology are encouraging options for future research. Thermoelectrics offer a promising cogeneration opportunity, and enhancements in TEM materials will improve the technology's potential. Recognizing and solving the remaining challenges of TEM system integration are required to improve overall system efficiency and power output.

Acknowledgements

We acknowledge the support of a NSF/DOE Partnership on Thermoelectric Devices for Vehicle Applications grant, a Precourt Energy Efficiency Center grant, and National Science Foundation Graduate

Research, Sandia National Labs, and Stanford's DARE fellowships. Discussions with Drs. Boris Kozinsky, Sungbae Park, Daehyun Wee, and Aleksandar Kojic of Bosch Research Corporation were very helpful in completing this work.

REFERENCES

[1] M. Zebarjadi, K. Esfarjani, M.S. Dresselhaus, Z.F. Ren, G. Chen. Perspectives on thermoelectrics: from fundamentals to device applications. Energy & Environmental Science. 5 (2012) 5147.

[2] T.M. Tritt. Thermoelectric Phenomena, Materials, and Applications. Annual Review of Materials Research. 41 (2011) 433-48.

[3] Federal Energy Regulatory Commission. The potential benefits of distributed generation and rate-related issues that may impede their expansion. in: U.S.D.O.E., (Ed.).2007.

[4] L.E. Bell. Cooling, heating, generating power, and recovering waste heat with thermoelectric systems. Science. 321 (2008) 1457-61.

[5] J.W. LaGrandeur, L.E. Bell, D.T. Crane. Recent Progress in Thermoelectric Power Generation Systems for Commercial Applications. Materials Research Society Symposium. Materials Research Society2011.

[6] M.D. Rowe, G. Min, S.G.K. Williams, A. Aoune, K. Matsuura, V.L. Kuznetsov, et al. Thermoelectric recoversy of waste heat - case studies. 32nd Intersociety Energy Conversion Engineering Conference1997.

[7] S. LeBlanc, Y. Gao, K.E. Goodson. Thermoelectric Heat Recovery from a Tankless Water Heating System. 2008 ASME International Mechanical Engineering Congress and Exposition, Boston, Massachusetts, 2008.

[8] A. Shakouri. Recent Developments in Semiconductor Thermoelectric Physics and Materials. Annual Review of Materials Research. 41 (2011) 399-431.

[9] D.T. Crane, G.S. Jackson. Optimization of cross flow heat exchangers for thermoelectric waste heat recovery. Energy Conversion and Management. 45 (2004) 1565-82.

[10] X. Niu, J. Yu, S. Wang. Experimental study on low-temperature waste heat thermoelectric generator. Journal of Power Sources. 188 (2009) 621-6.

[11] M.A. Karri, E.F. Thacher, B.T. Helenbrook. Exhaust energy conversion by thermoelectric generator: Two case studies. Energy Conversion and Management. 52 (2011) 1596-611.

[12] G.J. Snyder, E.S. Toberer. Complex thermoelectric materials. Nature Materials. 7 (2008).

[13] G.S. Nolas, J. Poon, M. Kanatzidis. Recent developments in buk thermoelectric materials. MRS Bulletin. 31 (2006).

[14] A.M. Pettes, M.S. Hodes, K.E. Goodson. Optimized thermoelectric refrigeration in the presence of thermal boundary resistance. IEEE Transactions on Advanced Packaging. 32 (2009).

[15] T. Tong, Y. Zhao, L. Delzeit, A. Kashani, M. Meyyappan, A. Majumdar. Dense vertically aligned multiwalled carbon nanotube arrays as thermal interface materials. IEEE Transactions on Components and Packaging Technologies. 30 (2007).

[16] M.A. Panzer, G. Zhang, D. Mann, X. Hu, E. Pop, H. Dai, et al. Thermal Properties of Metal-Coated Vertically Aligned Single-Wall Nanotube Arrays. Journal of Heat Transfer. 130 (2008) 052401.

[17] Y. Won, Y. Gao, M.A. Panzer, S. Dogbe, L. Pan, T.W. Kenny, et al. Mechanical characterization of aligned multi-walled carbon nanotube films using microfabricated resonators. Carbon. 50 (2012) 347-55.

[18] Y. Gao, A.M. Marconnet, M.A. Panzer, S. LeBlanc, S. Dogbe, Y. Ezzahri, et al. Nanostructured Interfaces for Thermoelectrics. Journal of Electronic Materials. 39 (2010) 1456-62.

[19] Y. Gao, T. Kodama, Y. Won, S. Dogbe, L. Pan, K.E. Goodson. Impact of nanotube density and alignment on the elastic modulus near the top and base surfaces of aligned multi-walled carbon nanotube films. Carbon. (2012).

[20] J. Fairbanks. Vehicular Thermoelectrics: A New Green Technology. in: D.o. Energy, (Ed.). 2011 Thermoelectrics Applications Workshop, San Diego, CA, 2011.

[21] T.J. Hendricks, W.T. Choate. Engineering scoping study of thermoelectric generator systems for industrial waste heat recovery. in: D.o. Energy, (Ed.).2006.

[22] G. Min, D.M. Rowe. Conversion efficiency of thermoelectric combustion systems. IEEE Transactions on Energy Conversion. 22 (2007).

[23] M. Chen, S.-S. Lu, B. Liao. On the Figure of Merit of Thermoelectric Generators. Journal of Energy Resources Technology. 127 (2005) 37.

[24] J. Esarte, G. Min, D.M. Rowe. Modelling heat exchangers for thermoelectric generators. Journal of Power Sources. 93 (2001).

[25] T.J. Hendricks. Thermal System Interactions in Optimizing Advanced Thermoelectric Energy Recovery Systems. Journal of Energy Resources Technology. 129 (2007) 223.

[26] R.B. Peterson. The Maximum Power Operating Point for a Combustion-Driven Thermoelectric Converter With Heat Recirculation. Journal of Engineering for Gas Turbines and Power. 129 (2007) 1106.

[27] D. Kraemer, B. Poudel, H.-P. Feng, J.C. Caylor, B. Yu, X. Yan, et al. High-performance flat-panel solar thermoelectric generators with high thermal concentration. Nature Materials. 10 (2011).

[28] F.P. Incropera, D.P. Dewitt, T.L. Bergman, A.S. Lavine. Fundamentals of Mass and Heat Transfer. McGraw-Hill, New York, 2007.

[29] Y. Pei, N.A. Heinz, A. LaLonde, G.J. Snyder. Combination of large nanostructures and complex band structure for high performance thermoelectric lead telluride. Energy & Environmental Science. 4 (2011) 3640.

[30] K. Yazawa, A. Shakouri. Cost-efficiency trade-off and the design of thermoelectric power generators. Environmental science & technology. 45 (2011) 7548-53.

[31] S. LeBlanc, S.K. Yee, M. Scullin, C. Dames, K.E. Goodson. Material and Manufacturing Cost Considerations for Thermoelectrics. 2012.

[32] M.A. McNeil, N. Bojda. Cost-effectiveness of high-efficiency appliances in the U.S. residential sector: A case study. Energy Policy. (2012).

[33] T.J. Hendricks, J.A. Lustbader. Advanced thermoelectric power system investigations for light-duty and heavy-duty applications: Part I. 21st International Conference on Thermoelectrics2002.

[34] T.J. Hendricks, J.A. Lustbader. Advanced thermoelectric power system investigations for light-duty and heavy-duty applications: Part II. 21st International Conference on Thermoelectrics2002.

[35] Bosch.

[36] N. Kloub. Improving the gas instantaneous water heaters performanc. American Journal of Applied Sciences. 2 (2005).

[37] G. Min, D.M. Rowe. Ring-structured thermoelectric module. Semiconductor Science and Technology. 22 (2007) 880-3.

[38] W.M. Kays, A.L. London. Compact Heat Exchangers. McGraw-Hill, New York, 1984.

[39] CRC Handbook of Thermoelectrics. CRC Press, Boca Raton, 1995.

[40] G. Snyder, T. Ursell. Thermoelectric Efficiency and Compatibility. Physical Review Letters. 91 (2003).

[41] R. Prasher. Thermal Interface Materials: Historical Perspective, Status, and Future Directions. Proceedings of the IEEE. 94.

[42] P.M. Mayer, R.J. Ram. Optimization of Heat Sink–Limited Thermoelectric Generators. Nanoscale and Microscale Thermophysical Engineering. 10 (2006) 143-55.

[43] K.E. Goodson. Automotive Thermoelectric Modules with Scalable Thermo- and Electro-Mechanical Interfaces. 2011 Thermoelectrics Applications Workshop. U.S. Department of Energy, San Diego, CA, 2011.